Electronic Supplementary Material (ESI) for Journal of Materials Chemistry A.

Supporting Information

Efficient Visible-Light-Driven Hydrogen Generation from Water Splitting Catalyzed by Highly Stable CdS@Mo_2C-C Core-Shell Nanorods

Sha-Sha Yi,[a,b] *Jun-Min Yan,*[a,b,*] *Ba-Ri Wulan,*[b] *and Qing Jiang*[b]

[a] State key laboratory of automotive simulation and control, Jilin University, Changchun, 130022, China.

[b] Key Laboratory of Automobile Materials (Jilin University), Ministry of Education, Department of Materials Science and Engineering, Jilin University, Changchun, 130022, China.

[*] Corresponding author: junminyan@jlu.edu.cn

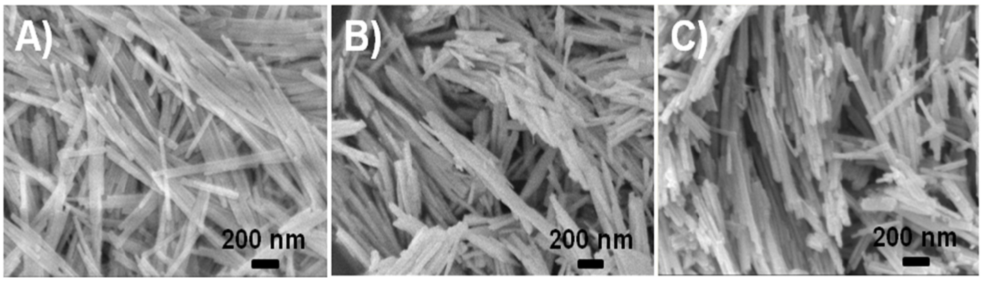

Fig. S1 FESEM images of A) pure CdS NRs, B) CdS@1Mo_2C-C core-shell NRs, and C) CdS@5Mo_2C-C core-shell NRs.

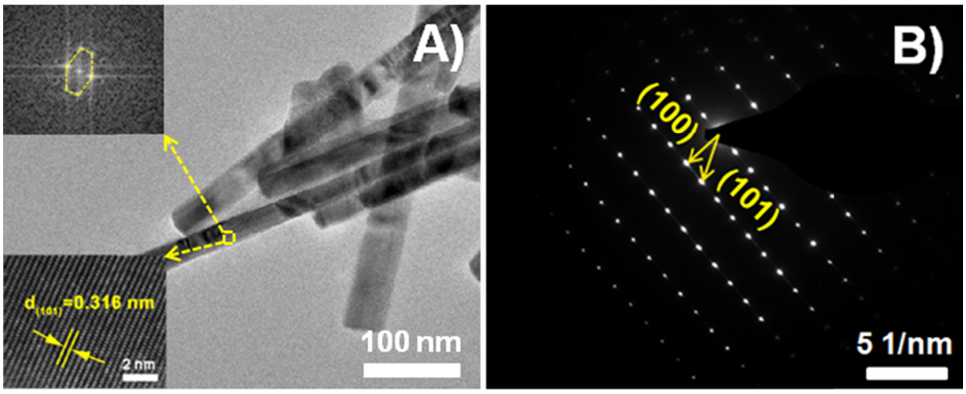

Fig. S2 A) TEM image of CdS NRs, inset: FFT pattern and HRTEM image of CdS NRs, and B) SAED pattern of CdS NRs.

As shown in Fig. S2A, several smooth NRs are observed for CdS with its spacing of 0.316 nm corresponded to the (101) plane (Fig. S2A, inset). The Fourier transform (FFT) pattern confirms the hexagonal CdS structure (Fig. S2A, inset). The selected area electron diffraction (SAED) pattern acquired from an ensemble CdS NRs presents the ordered diffraction spots, indicating the single crystalline nature of CdS (Fig. S2B).

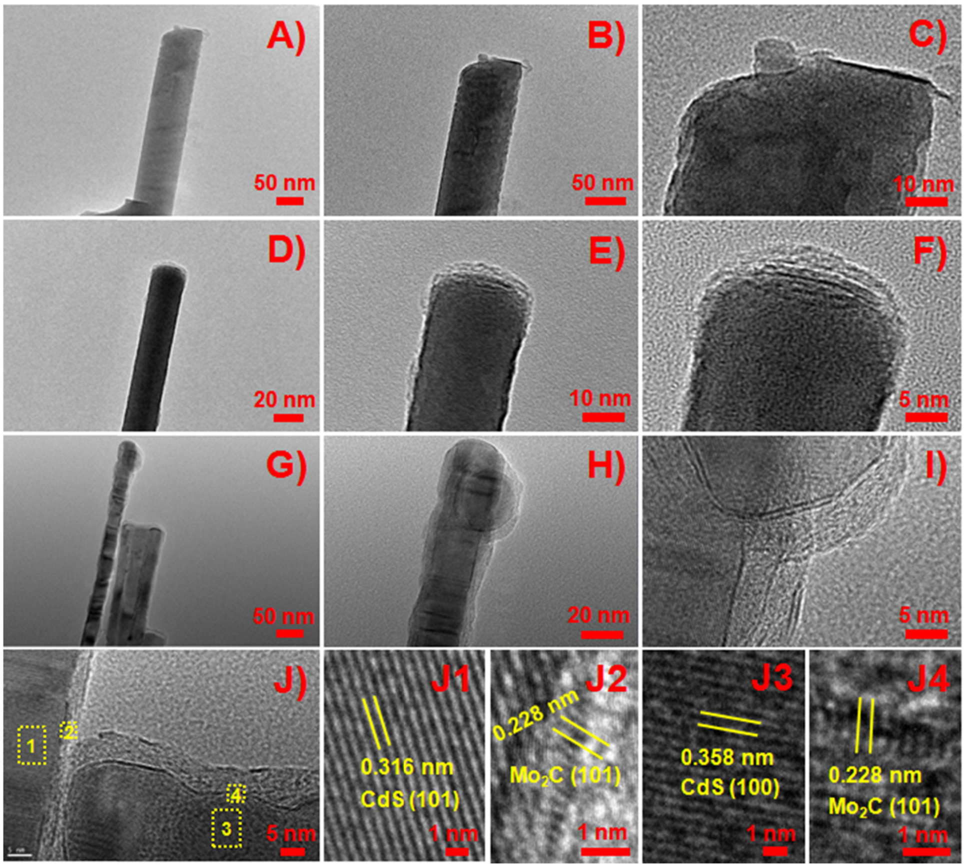

Fig. S3 TEM images for (A, B, C) CdS@0.5Mo_2C-C, (D, E, F) CdS@2Mo_2C-C, and (G, H, I) CdS@5Mo_2C-C core-shell NRs; TEM (J) and the related HRTEM (J1-J4) images of the circled areas for CdS@5Mo_2C-C.

Fig. S3 shows the typical TEM and HRTEM images of CdS@0.5Mo_2C-C, CdS@2Mo_2C-C, and CdS@5Mo_2C-C core-shell NRs. It is clear that the nanolayer out of CdS is become thicker with the increased addition of Mo_2C-C in CdS@xMo_2C-C system. In Fig. S3(J, and J1-J4), the circled areas of 1 and 3 distinctly reveal two kinds of lattice fringes of 0.316 and 0.358 nm, which are corresponded well to the (101) and (100) planes of CdS (Fig. S2B), respectively. And the lattice spacing at the interlayer (framed areas of 2 and 4) Mo_2C is 0.228 nm, which is in accordance with the (101) plane of Mo_2C.

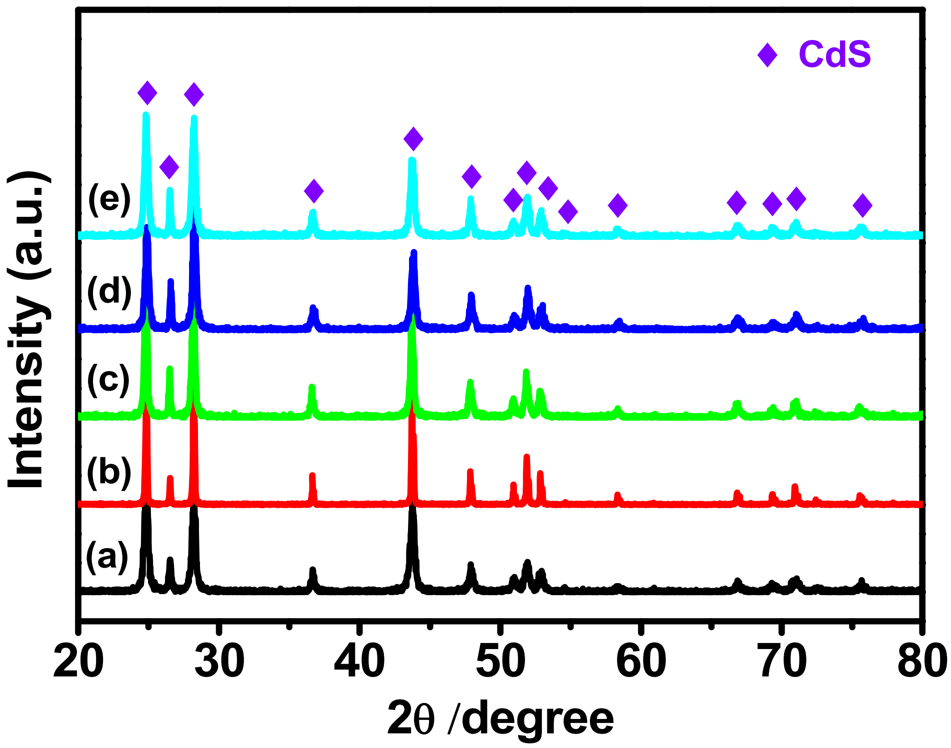

Fig. S4 XRD patterns of (a) CdS, (b) CdS@0.5Mo_2C-C, (c) CdS@1Mo_2C-C, (d) CdS@2Mo_2C-C, and (e) CdS@5Mo_2C-C.

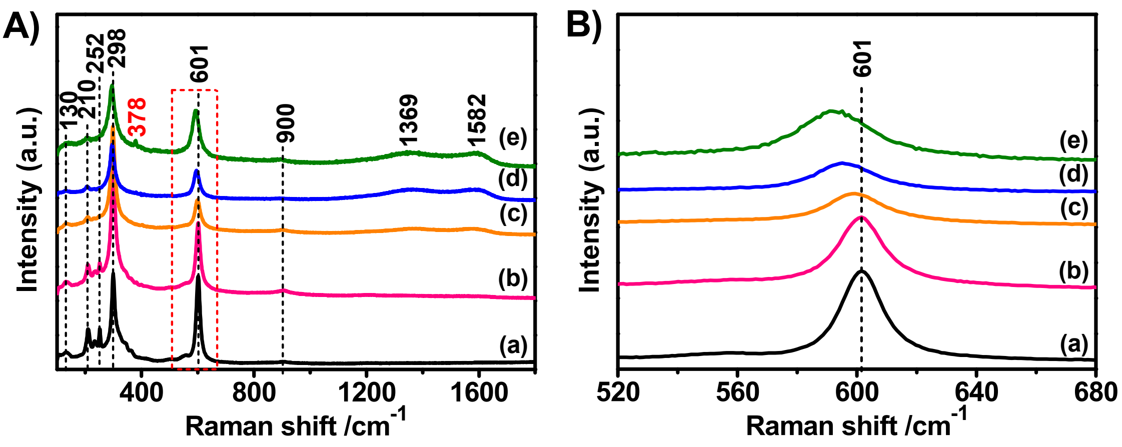

Fig. S5 A) Raman spectra and B) the enlarged view of the red circled area of (a) CdS, (b) CdS@0.5Mo_2C-C, (c) CdS@1Mo_2C-C, (d) CdS@2Mo_2C-C, and (e) CdS@5Mo_2C-C.

The Raman signal at 378 cm^{-1} is observed for CdS@5Mo_2C-C (Fig. S5A), which can be ascribed to Mo_2C,[S1] suggesting the existence of Mo_2C in the CdS@5Mo_2C-C compound.

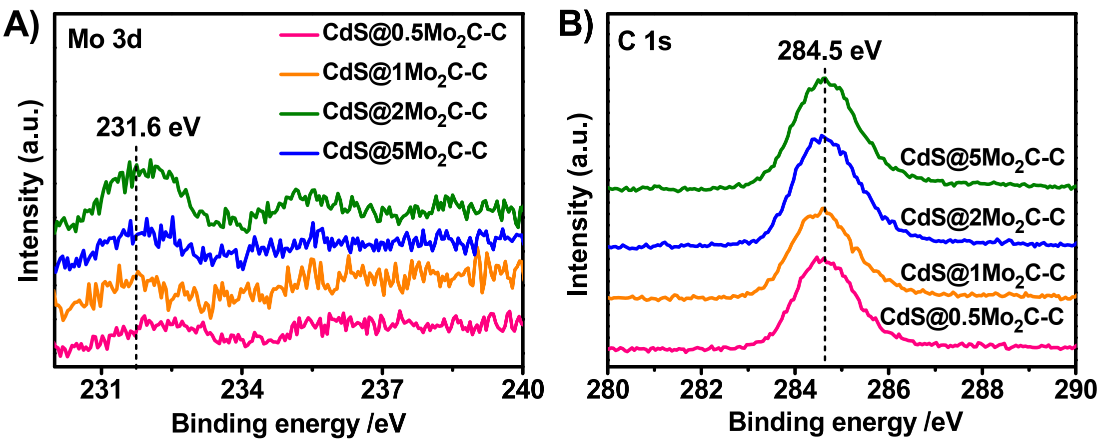

Fig. S6 XPS spectra of A) Mo 3d and B) C 1s for CdS and CdS@xMo_2C-C (x = 0.5, 1, 2, and 5).

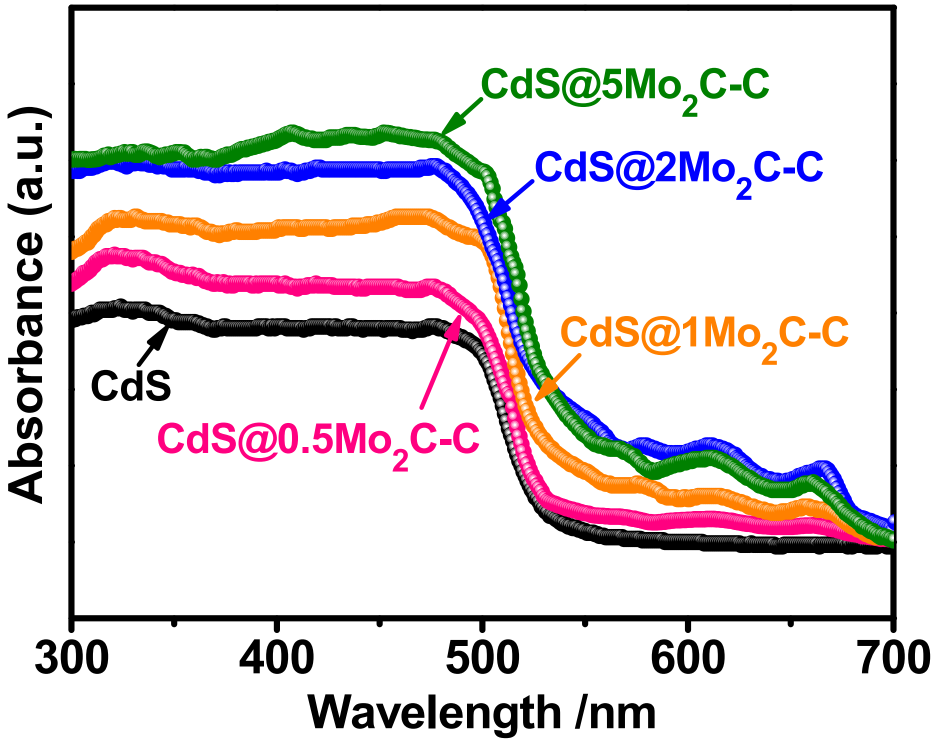

Fig. S7 UV-vis DRS of CdS, and CdS@xMo_2C-C (x = 0.5, 1, 2, and 5).

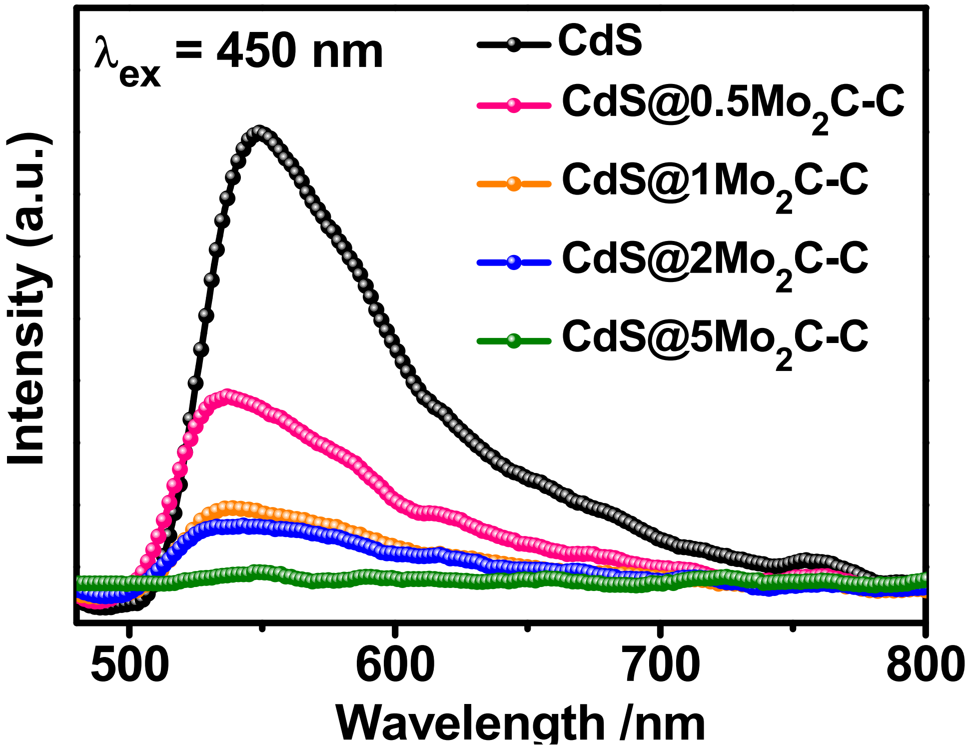

Fig. S8 PL spectra of CdS, and CdS@xMo_2C-C (x = 0.5, 1, 2, and 5).

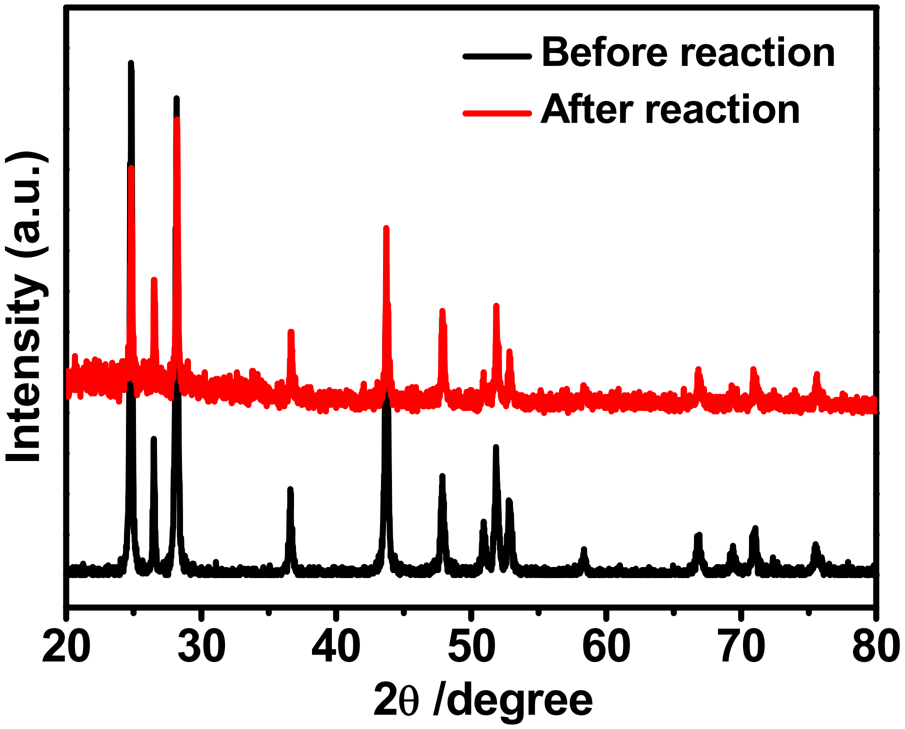

Fig. S9 XRD patterns for CdS@1Mo_2C-C before and after photocatalytic recycling runs.

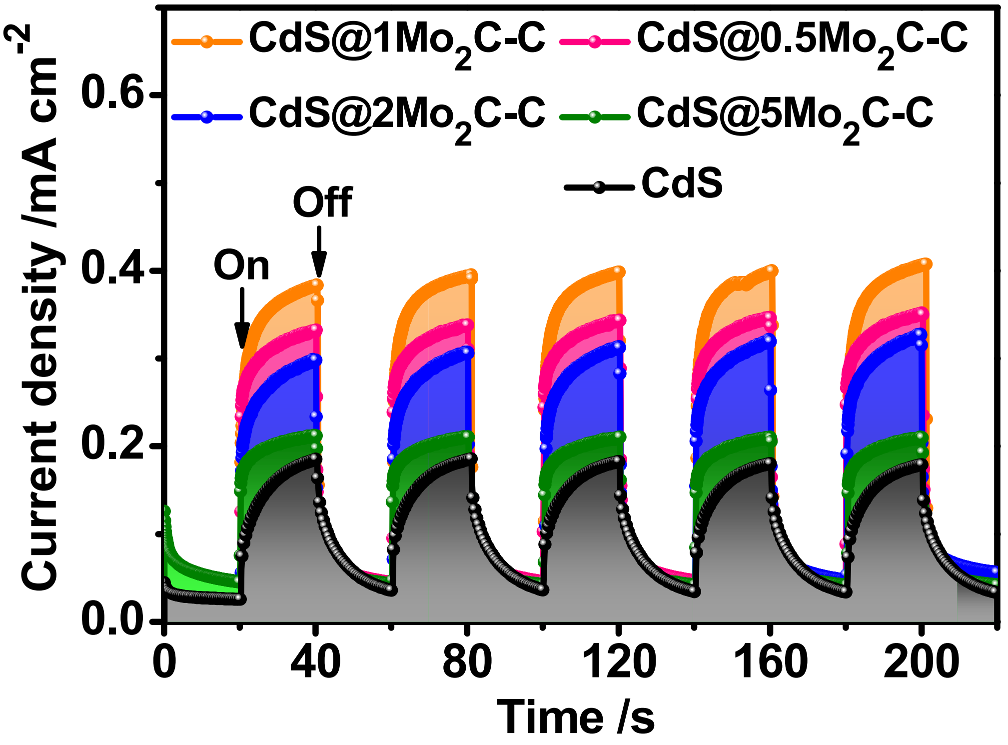

Fig. S10 Transient photocurrent responses at 0 V *vs.* Ag/AgCl over CdS, and CdS@xMo$_2$C-C (x = 0.5, 1, 2, and 5) under visible light irradiation (λ ≥ 420 nm).

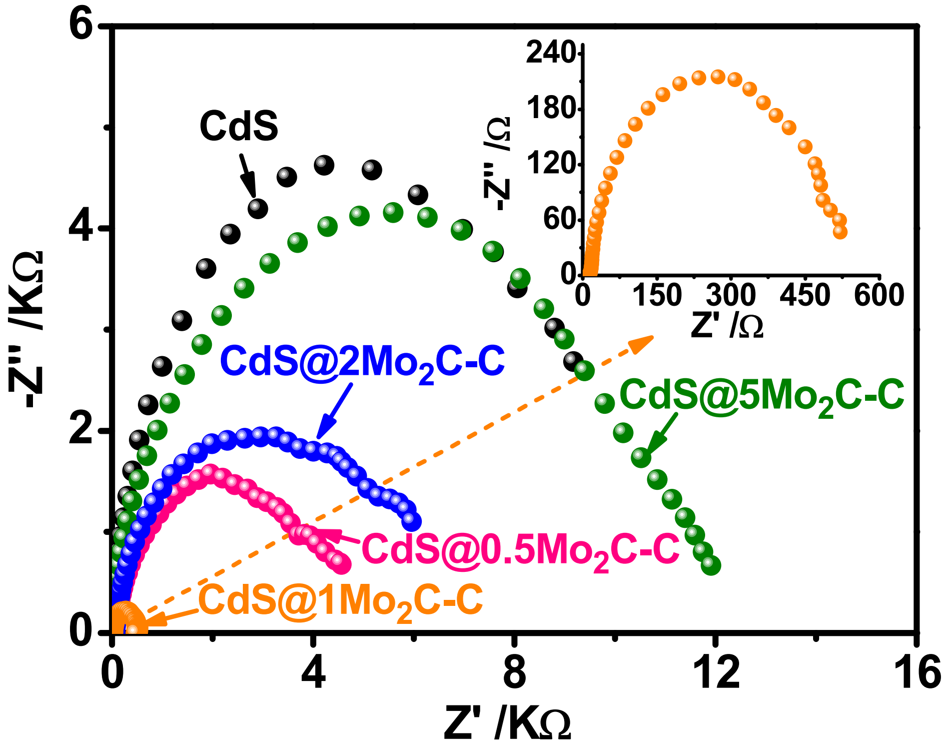

Fig. S11 EIS Nyquist plots of CdS and CdS@xMo_2C-C (x = 0.5, 1, 2, and 5) under visible light irradiation (λ ≥ 420 nm).

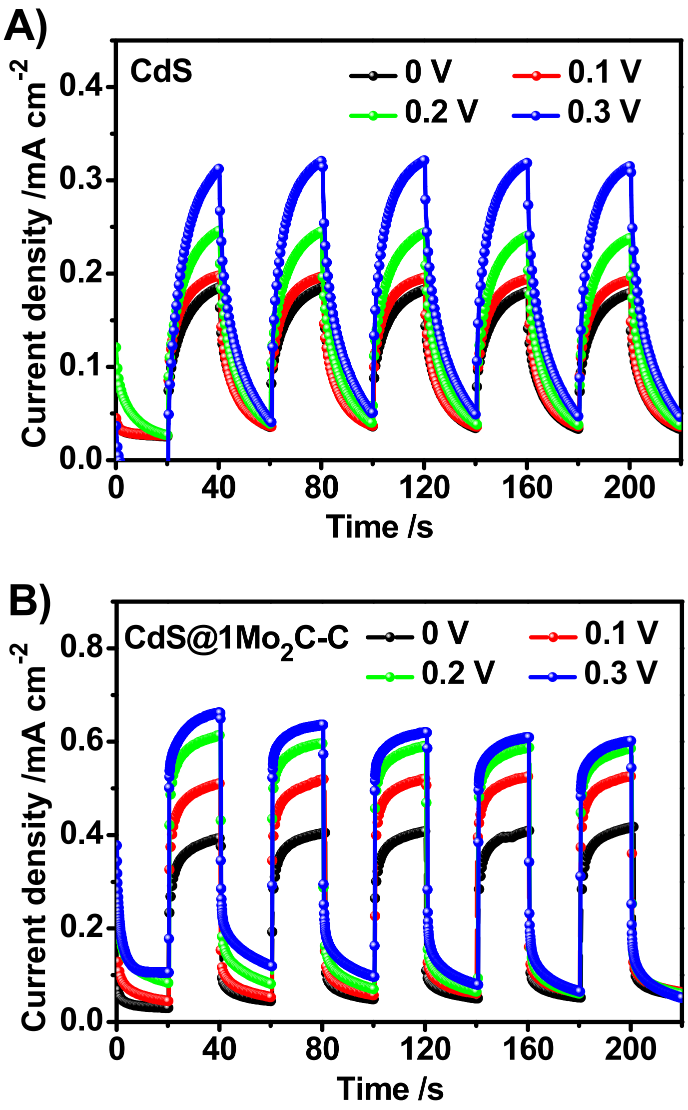

Fig. S12 Transient photocurrent responses over A) CdS, and B) CdS@1Mo$_2$C-C with various applied bias potentials (V *vs.* Ag/AgCl) under visible light irradiation (λ ≥ 420 nm).

The transient photocurrent responses over pure CdS and CdS@1Mo$_2$C-C with various applied bias potentials (V *vs.* Ag/AgCl) under visible light irradiation (λ ≥ 420 nm) are shown in Fig. S12. Clearly, when the irradiation is switched on, the photocurrent response for pure CdS is slowly increased, while sharply increased for CdS@1Mo$_2$C-C; similarly, when the irradiation is switched off, the photocurrent is rapidly dropped to dark state for CdS@1Mo_2C-C, while not the case for pure CdS. These results can be attributed to the fact that the addition of Mo_2C-C nanolayers can effectively speed up the charge transfer and suppress their recombination to some extent.

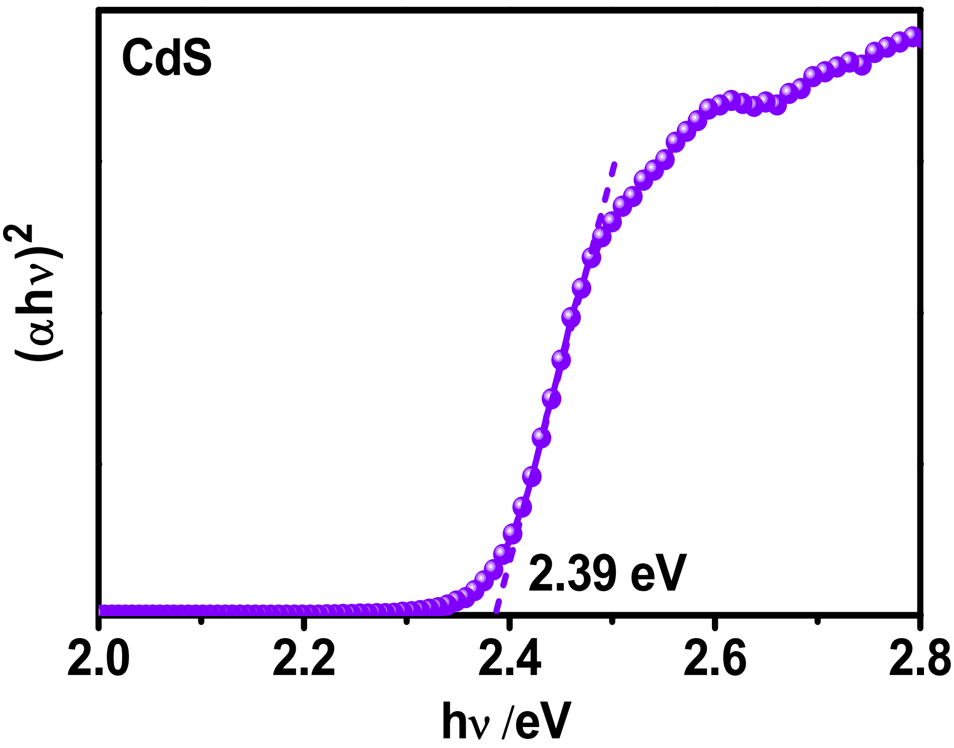

Fig. S13 Plots of the $(\alpha h\nu)^2$ *vs* photon energy (hν) for pure CdS.

The band gap (E_g) of pure CdS is determined to be 2.39 eV by employing the functional equation: $(\alpha h\nu)^n = A(h\nu - E_g)$,[S2] where α is the absorption coefficient, hν is the incident photon energy, and n is 2, which depends on the transition type in the semiconductor (2 for direct transition, and 1/2 for indirect transition).[8]

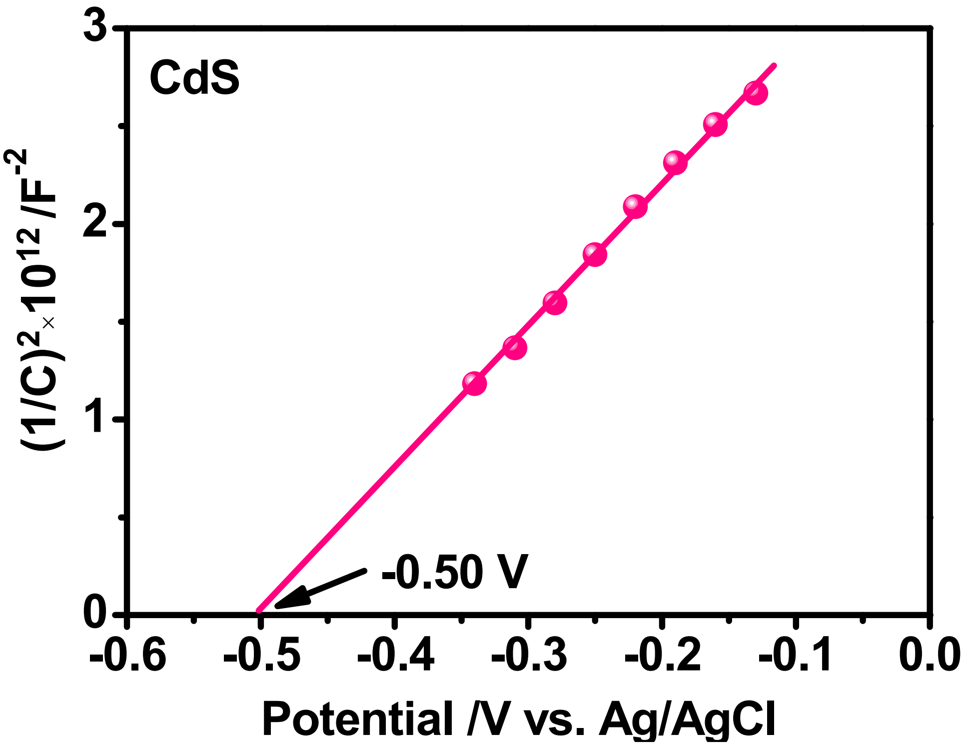

Fig. S14 M-S plots for pure CdS sample.

The flat band potentials of CdS can be determined by the Mott-Schottky equation as below: [S3-S5]

$$1/C^2 = (2/e\varepsilon_0\,\varepsilon N_a)[(V - V_{FB}) - kT/e]$$

where C, ε_0, ε, e, V, K, T, and N_a are the capacitance of the space charge region, vacuum permittivity, dielectric constant of CdS, electron charge, electrode applied potential, k Boltzmann constant, absolute temperature, and acceptor concentration, respectively. The temperature term is generally small and can be neglected. According to the Mott-Schottky equation, a linear relationship of C^{-2} *vs*. V can be observed. The flat band potential for CdS is estimated to be -0.50 V *vs*. Ag/AgCl.

Obviously, CdS shows the positive slope for the M-S plots, confirming that CdS is a n-type semiconductor.[S4] Considering the small difference between the flat band potential and the lower conduction band (CB) edge for n-type semiconductors,[S5,S6] the CB potential for CdS is roughly valued to be -0.50 V versus normal hydrogen electrode (NHE). Additionally, the valence band (VB) of CdS is 1.89 V *versus* NHE calculated by the equation: $E_{VB} = E_{CB} + E_g$.[64]

Table S1. Comparison of photocatalytic H_2 generation rates of CdS-based photocatalysts.

Photocatalyst	**Electron donor**	**Light source**	**H_2 (μmol h^{-1} g^{-1})**	**Ref.**
NiS/Te/CdS	Lactic acid	300 W Xe ($\lambda \geq 420$ nm)	1033	30
$CdS/Pt/WO_3$	Lactic acid	500 W Xe ($\lambda \geq 400$ nm)	2900	12
MoS_2/CdS	Na_2S-Na_2SO_3	300 W Xe ($\lambda \geq 420$ nm)	2014	16
Au/CdS	Na_2S-Na_2SO_3	300 W Xe ($\lambda \geq 400$ nm)	7300	44
$RGO/Zn_{0.8}Cd_{0.2}S$	Na_2S-Na_2SO_3	Solar light	1824	23
$Ni_2S/RGO/Zn_{0.8}Cd_{0.2}S$	Na_2S-Na_2SO_3	Solar light	4790	41
$CdS/Au/SrTiO_3(Pt)$	Na_2S-Na_2SO_3	300 W Xe ($\lambda \geq 420$ nm)	1091	45
ZnS-(CdS/Au)	Na_2S-Na_2SO_3	Solar light	1825	46
WS_2/CdS	Lactic acid	300 W Xe ($\lambda \geq 420$ nm)	4200	47
$Ni(OH)_2/CdS$	Triethanolamine	300 W Xe ($\lambda \geq 420$ nm)	5084	48
$Au@TiO_2$-CdS	Na_2S-Na_2SO_3	300 W Xe ($\lambda \geq 420$ nm)	2000	49
CdS/Au/ZnO	Na_2S-Na_2SO_3	Solar light	600	50
C_{60}-CdS/TiO_2	Na_2S-Na_2SO_3	LED ($\lambda \geq 420$ nm)	121	51
Au/CdS	Na_2S-Na_2SO_3	500 W Warrior WEHL halogen bulb lamp	10800	52
Au/CdS/Pt	Na_2S-Na_2SO_3	300 W Xe ($\lambda \geq 420$ nm)	11500	53
MoS_2/RGO-CdS	Na_2S-Na_2SO_3	300 W Xe ($\lambda \geq 420$ nm)	9000	4
$CdS@Mo_2C$-C	Na_2S-Na_2SO_3	300 W Xe ($\lambda \geq 420$ nm)	17240	This work

References

S1 M. L. Frauwallner, F. Lopez-Linares, J. Lara-Romero, C. E. Scott, V. Ali, E. Hernandez and P. Pereira-Almao, *Appl. Catal. A: General*, 2011, **394**, 62.

S2 M. Butler, *J Appl. Phys.*, 1977, **48**, 1914.

S3 T. F. Jiang, T. F. Xie, L. P. Chen, Z. W. Fu and D. J. Wang, *Nanoscale*, 2013, **5**, 2938.

S4 A. G. Hufnagel, K. Peters, A. Muller, C. Scheu, D. F. R. Ng and T. Bein, *Adv. Funct. Mater.*, 2016, **26**, 4435.

S5 X. Li, J. Yu, J. Low, Y. Fang, J. Xiao and X. Chen, *J. Mater. Chem. A*, 2015, **3**, 2485.

S6 S. J. Hong, S. Lee, J. S. Jang and J. S. Lee, *Energy Environ. Sci.*, 2011, **4**, 1781.